SDR BASED AGILE RADIOMETER WITH ONBOARD RFI PROCESSING ON A SMALL UAS

Md Mehedi Farhad, Sabyasachi Biswas, A. M. Alam, Ali C. Gurbuz, and Mehmet Kurum

Mississippi State University, Department of Electrical and Computer Engineering, Mississippi State, MS, 39762, USA

ABSTRACT

Passive microwave remote sensing plays an essential role in providing valuable information about the Earth's surface, particularly for agriculture, water management, forestry, and other environmental fields. One of the key requirements for precision agricultural applications is the availability of fieldscale high-resolution remote sensing data products. With the recent development of reliable unmanned aircraft systems (UAS), airborne deployment of remote sensing sensors has become more widespread to provide such products. With this in mind, we developed a UAS-based dual H-pol (horizontal) and V-pol (vertical) polarized radiometer operating in L-band (1400-1427 MHz). The custom dual-polarized antenna acquires surface emission response through a softwaredefined radio (SDR). This SDR-based system provides full control over the data acquisition parameters such as bandwidth, sampling frequency, and data size. Radio frequency interference (RFI) poses a significant challenge in radiometric measurements, requiring post-processing of the full-band radiometer data to identify and eliminate RFI-contaminated measurements, thus ensuring accurate Earth emission readings.. In this paper, we implemented near-real-time RFI detection onboard during the flight to accelerate the postprocessing. The altitude and the speed of the UAS can be varied to achieve desired ground resolution for the measurement. This paper presents the full custom design and development of a lightweight SDR-based UAS-borne radiometer for precision agriculture. Additionally, we introduce the concept of an agile radiometer implemented from a small UAS that can serve as a testbed for both current and future spaceborne missions.

Index Terms— SDR, Radiometer, RFI, UAS, microwave, L-band, b210, dual-polarized, passive, coexistence, soil moisture.

1. INTRODUCTION

The concept of L-band (1400-1427 MHz) microwave radiometry is to measure the brightness temperature (BT) to retrieve the earth's surface geophysical parameters [1] such



Fig. 1. Radiometer integrated on a custom UAS.

as soil moisture, vegetation optical depth, sea surface salinity, snow density, sea ice thickness, and snow liquid water. The most notable spaceborne L-band radiometers to measure different environmental parameters are the European Space Agency (ESA)'s Soil Moisture and Ocean Salinity Satellite (SMOS) [2] and the National Aeronautics and Space Administration (NASA)'s Aquarius and Soil Moisture Active Passive (SMAP) [3] missions. However, RFI from various active services, such as communications systems and radars, impacts recent measurements made by spaceborne L-band radiometers [4,5]. These missions experienced significant RFI contamination that can cause significant data loss and measurement errors in both space and time and reduce the scientific value of the data obtained. To investigate this scenario in a controlled environment, a unique testbed has been design and built for verification, and optimization of active/passive coexistence in real-world settings in [6].

The implementation of L-band radiometers on a UAS platform has been studied in a few published works with various capabilities. For instance, in [7], the authors have designed a compact, portable radiometer with onboard two-port calibration and the capability of integrating on a small

This work was supported by National Science Foundation (NSF) Grant # 2030291.

copter. In [8], the authors used a software-defined radio (SDR), USRP ETTUS N-200, to design and implement a radiometer from a tower-based platform. The distinct contribution of this paper can be summarised as follows: (1) this study presents a highly compact SDR-based dual polarized radiometer, (2) this radiometer is highly-adaptive with the ability to sample the entire 27 MHz bandwidth, and (3) the near-real-time processing of data allows faster detection of RFI onboard the UAS. The following sections will briefly describe the design, implementation, calibration, system performance, and finally, the summary and future work.

2. DESIGN AND IMPLEMENTATION

Fig. 1 shows a picture of our recently developed L-band radiometer attached to a UAS (hexacopter) with a dual-polarized antenna. This section describes the radiometer design principle, data acquisition process, and radiometric calibration to calculate the BT from raw antenna count measurement.

2.1. Design Schematic

This dual (H-pol and V-pol) polarized radiometer operates based on direct detection architecture and is divided into two sections, radio frequency (RF)-front-end and back-end processing. The RF front-end consists of a 4-port RF switch followed by a 20 dB isolator, a custom bandpass filter (BPF), and a low noise amplifier (LNA). The H-pol and V-pol antennas are connected to the 2-port of the RF switch. The other two ports of the RF-switch are connected to 50 ohms matched load, serving as a hot source (HS), and a reverse LNA terminated with 50 ohms matched load, serving as an active cold source (ACS). To ensure temperature stability, all the RF components are placed on a temperature-controlled aluminum plate. The back end of the radiometer consists of an SDR (USRP B210), an Intel mini-PC (NUK), and two Raspberry Pi4s. A schematic of the radiometer design is given in Fig. 2. The front-end compensates for temperature drifts as the radiometer performs calibration with its internal HS and ACS for each measurement cycle. During each cycle, the radiometer records raw data from each port of the RF switch for 250 ms, having a 1000 ms integration time, while utilizing 27-MHz full bandwidth.

The radiometer is designed in a multilayer structure and enclosed inside a compact box. The whole box is covered with a thin layer of metal tape to isolate the internal instrument from outside RFI. Different layers of the radiometer, as well as the overall response of the system, are displayed in Fig. 3. The first layer holds all the RF equipment, while the second and third layers accommodate the SDR, electromechanical relays, raspberry Pi4s, and temperature controller. The whole radiometric S_{21} response was measured with a network analyzer and shown in Figure 3[d].

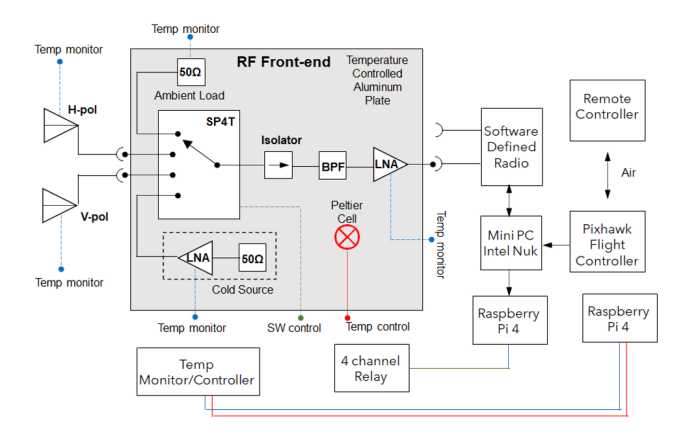


Fig. 2. Radiometer schematic diagram.

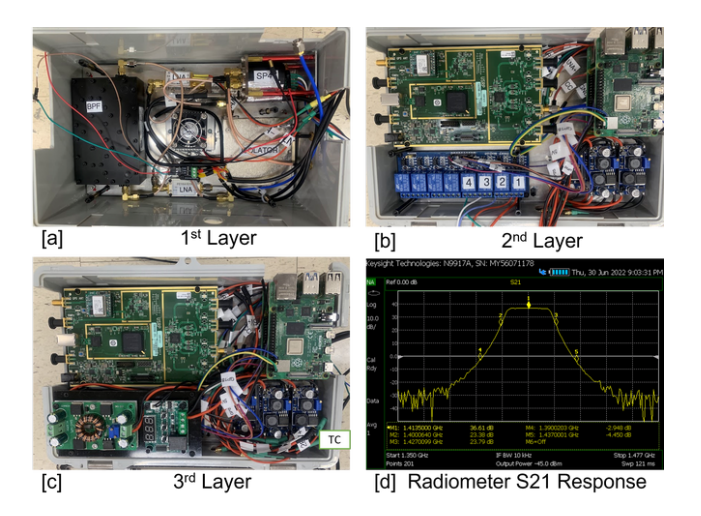


Fig. 3. Radiometer enclosed in a small box with multi-layer structure. Three layers are represented in [a], [b], and [c], and [d] is the total radiometric response measured with network analyzer

2.2. Antenna Design and Characterization

A dual-polarized air-gap patch microwave (2×2) array antenna is designed and fabricated using chemical etching. The antenna has virtually no side lobes and negligible back lobes, with a realized gain of 12.84 dB. The return loss (S_{11}) of \sim -30 dB for both polarization is achieved in a simulated environment. The antenna has a beamwidth of 37° . Both antennas are characterized in the anechoic chamber using a vector network analyzer. Fig. 4 represents the 3D radiation pattern and the simulated and measured return loss (S_{11}) of both antennas.

2.3. Calibration

The calibration of the radiometer is a crucial step in converting the raw antenna count (Inphase and Quadrature) samples into BT. It is common to utilize a two-port internal calibration with the HS and ACS. However, it is nescessary to calibrate

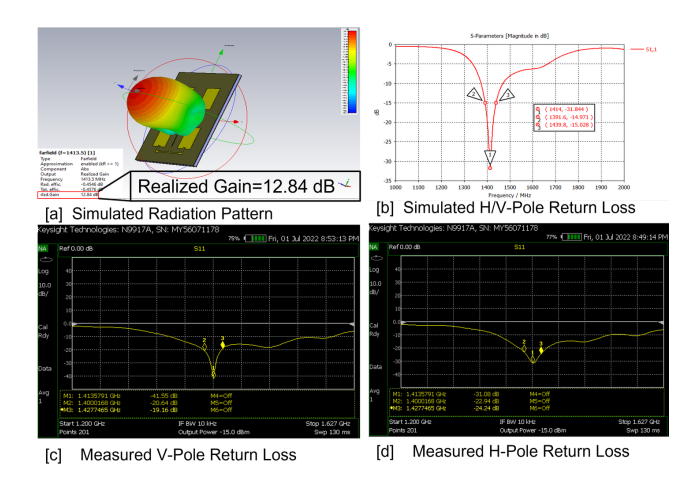


Fig. 4. [a] radiometer dual-polarized antenna 3D radiation pattern, [b] simulated antenna return loss, [c] measured Return loss (V-pol), and [d] measured return loss (H-pol)

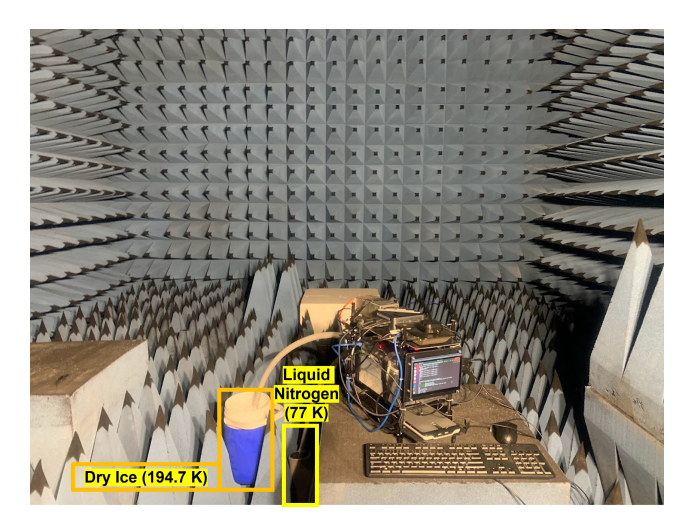


Fig. 5. Radiometer internal calibration setup using liquid nitrogen (77K) and dry ice (194.7K) in the anechoic chamber.

the ACS BT to utilize the two-port internal calibration. To calibrate the ACS, we used two known sources: liquid nitrogen (LN), having a temperature of 77K, and dry ice (DI) of 194.7K. The radiometer uses HS and ACS BT at each second simultaneous with H-pol and V-pol antenna counts to calculate the BT of the target object. Fig. 5 shows the internal calibration setup with LN and DI.

The RMS voltage and the noise source temperature are linearly related to each other. 50 sets of data, where each set consisting of 9 data cycles, has been collected using LN on the H-pol port and DI on the V-pol port with varying radiometer's internal temperature (HS) from 293.15K to 300.15K. The temperature control sensors are attached with each of the components to measure their temperature at each time step and check the overall system temperature along with the effect of temperature change in the internal components of the

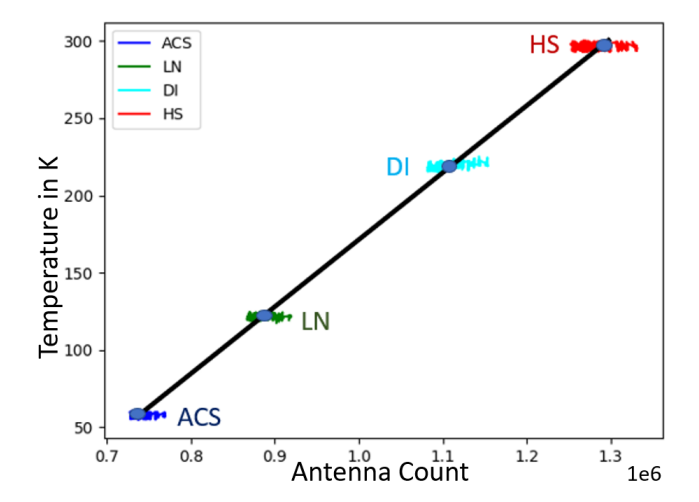


Fig. 6. Radiometer internal calibration linearity test.

radiometer. The radiometer collects data for 250 ms from each port during 1000 ms of data acquisition from H-pol, V-pol, HS, and ACS ports. Using this response from each cycle (1000 ms), a BT of ACS is calculated (55K to 59K) over about 8°C ambient temperature change and plotted with respect to the uncleaned raw power. Fig. 6 represents the linear relationship of ACS with LN, DI and HS.

3. SYSTEM PERFORMANCE

The radiometer has been fully tested in an anechoic chamber. We took several measurements and looked into the spectrogram results of the received data. After analyzing the spectrograms, we found some very interesting signal signatures in the frequency domain. In the protected L-band (1400-1427MHz), theoretically, there should not be any RFI while tested in the anechoic chamber. However, a computer monitor was required during the data collection process, which was placed just beside the radiometer setup. The monitor generated a signal at 1410 MHz inside the protected band. The signal was strong enough to be observed in the spectrogram plots. In Fig. 7(a), we can see 4 states of the radiometer response at H-pol, V-pol, HS, and ACS. But in the first 400ms, the monitor was turned on, and we can see the effect of the monitor very clearly. To protect the radiometer from the RFI, we covered the whole radiometer box with thin metal tape and turned off all nearby electronic devices during the data collection process.

3.1. Anechoic Chamber Absorber Test

The radiometer is placed in the anechoic chamber to measure the ambient temperature of the electromagnetic absorbers through the dual-polarized antenna. The radiometer's internal temperature is set to 20°C / 293.15K, which is the ambient temperature of the anechoic chamber. Fig. 7(b) represents

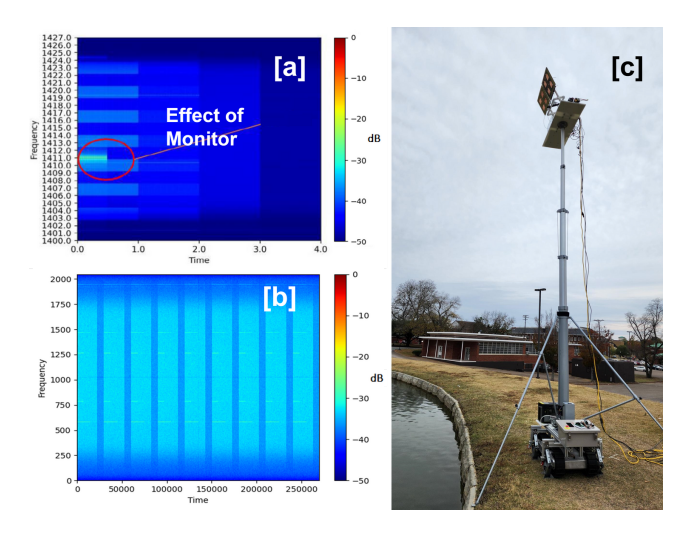


Fig. 7. [a] Radiometer internal component interference detection and mitigation, [b] spectrogram while radiometer placed inside the anechoic chamber, and [c] radiometer placed on a tower looking towards the water at 45° angle

the 9 cycle spectrogram of anechoic chamber measurement, where each cycle (1000 ms) represents the measurement of 4-port (H-pol, V-pol, HS and ACS), 250 ms each port. Here, the H-pol, V-pol and HS show the same antenna count, as all three ports observe the same ambient temperature inside the chamber. The white lines along the x-axis in Fig. 7(b) are the instrument generated RFI that need to be cleaned before converting the raw antenna count to the BT. The clean spectrogram and target source BT will be presented in the conference.

3.2. Water and Sky Test

For radiometer external calibration, data has been collected for sky, and water. At first, the radiometer's ACS and HS temperatures are checked. From the calculated ACS and HS temperature, a linearity curve is generated. External calibration is required to accurately measure the antenna effect on the target source's measurement and corresponding brightness temperature. In this case, the antenna is looking towards the water at 45 $^{\circ}$ angle. Figure. 7(c) represents the hardware setup for external calibration near Eckies Pond, located on the southeast part of the Mississippi State University campus. The same setup was used to get sky measurement by pointing the antenna towards the sky at a 0° angle. All the measurement data are still under post-processing. The result will be presented in the conference.

4. CONCLUSION AND FUTURE WORK

The compact radiometer is built to operate in the protected L band (1400-1427 MHz). The custom dual-polarized antenna is designed and fabricated. The radiometer is SDR-based, records full 27 Mhz bandwidth of data with a 30 MHz sampling

rate. The radiometer is capable of processing the data in nearreal time while flying and collecting data onboard the UAS. Multiple linearity test has been conducted in different ambient temperature environment. The radiometer has been attached underneath a custom UAS (Hexacopter) and successfully completed the flight test. For future work, the radiometer will be starting its data collection flight soon.

5. REFERENCES

- [1] Eryan Dai, Aravind Venkitasubramony, Albin Gasiewski, Maciej Stachura, and Jack Elston, "High spatial soil moisture mapping using small unmanned aerial system," in 2018 IEEE International Geoscience and Remote Sensing Symposium, 2018, pp. 6496–6499.
- [2] Y.H. Kerr, P. Waldteufel, J.-P. Wigneron, J. Martinuzzi, J. Font, and M. Berger, "Soil moisture retrieval from space: the soil moisture and ocean salinity (SMOS) mission," *IEEE Transactions on Geoscience and Remote* Sensing, vol. 39, no. 8, pp. 1729–1735, 2001.
- [3] Dara Entekhabi, Eni Njoku, Peggy O'Neill, Michael Spencer, Tom Jackson, Jared Entin, Eastwood Im, and Kent Kellogg, "The soil moisture active/passive mission (SMAP)," in 2008 IEEE International Geoscience and Remote Sensing Symposium, 2008, vol. 3, pp. 1 4.
- [4] Priscilla N Mohammed, Mustafa Aksoy, Jeffrey R Piepmeier, Joel T Johnson, and Alexandra Bringer, "SMAP L-band microwave radiometer: RFI mitigation prelaunch analysis and first year on-orbit observations," *IEEE Transactions on Geoscience and Remote Sensing*, vol. 54, no. 10, pp. 6035–6047, 2016.
- [5] Ahmed Manavi Alam, Mehmet Kurum, and Ali C. Gurbuz, "Radio frequency interference detection for SMAP radiometer using convolutional neural networks," *IEEE Journal of Selected Topics in Applied Earth Observations and Remote Sensing*, vol. 15, pp. 10099–10112, 2022.
- [6] Md Mehedi Farhad, Sabyasachi Biswas, Mohammad Abdus Shahid Rafi, Mehmet Kurum, and Ali C Gurbuz, "Design and implementation of a software defined radiobased radiometer operating from a small unmanned aircraft systems," in 2022 IEEE USNC-URSI Radio Science Meeting (Joint with AP-S Symposium). IEEE, 2022, pp. 17–18.
- [7] Derek Houtz, Reza Naderpour, and Mike Schwank, "Portable l-band radiometer (PoLRa): Design and characterization," *Remote Sensing*, vol. 12, no. 17, 2020.
- [8] Matthew Erik Nelson, "Implementation and evaluation of a software defined radio based radiometer," M.S. thesis, Iowa State University, 2016.